

Interplay of non-standard interactions and Earth's composition in atmospheric neutrino oscillations

Juan Carlos D'Olivo^{*1,2}, José Arnulfo Herrera Lara^{†1}, Ismael Romero^{‡2}, Matias Reynoso^{§2}, and Oscar A. Sampayo^{¶2}

¹*Instituto de Ciencias Nucleares, Universidad Nacional Autónoma de México, Circuito Exterior, Ciudad Universitaria, 04510 CDMX, Mexico.*

²*Instituto de Física de Mar del Plata (IFIMAR), CONICET, UNMDP, Departamento de Física, Universidad Nacional de Mar del Plata, Funes 3350, (7600) Mar del Plata, Argentina*

Abstract

Many geophysical and geochemical phenomena in the Earth's interior are related to physical and chemical processes in the outer core and the core-mantle boundary, directly linked to isotopic composition. Determining the composition using standard geophysical methods has been a challenge. The oscillations of atmospheric neutrinos, influenced by their weak interactions with terrestrial matter, offer a new way to gather valuable information about the Earth's internal structure and, in particular, to constrain the core composition. If neutrinos had as yet unknown non-standard interactions (NSI), this could affect their propagation in matter and consequently impact studies of Earth's composition using neutrino oscillation tomography. This study focuses on scalar-mediated NSI and their potential impact on atmospheric neutrino oscillations, which could obscure information about the hydrogen content in the outer core. In turn, compositional uncertainties could affect the characterization of NSI parameters. The analysis is based on a Monte-Carlo simulation of the energy distribution and azimuthal angles of neutrino-generated μ events. Using a model of the Earth consisting of 55 concentric shells with constant densities determined from the PREM, we evaluate the effect on the number of events due to changes in the outer core composition $(Z/A)_{oc}$ and the NSI strength parameter ϵ . To examine the detection capability to observe such variations, we consider regions in the plane of $(Z/A)_{oc}$ and ϵ where the statistical significance of the discrepancies between the modified Earth model and the reference model is less than 1σ .

1 Introduction

The seismic studies indicate that the Earth has a layered spherical structure in the form of concentric shells with increasing density as we go deeper to the core. From the analysis of iron meteorites and

*email: dolivo@nucleares.unam.mx

†email: fis_pp@ciencias.unam.mx

‡email: ismaelromero@hotmail.com

§email: matiasreynoso@gmail.com

¶email: sampayo@mdp.edu.ar

the observation of the planet’s moment of inertia, it is known that the Earth’s core is composed primarily of an iron-nickel alloy, with Ni/Fe ~ 0.06 . Two well-differentiated regions have been identified: the inner and outer core, distinguished by an abrupt density difference of 4.5% at a depth of approximately 5100 km [1]. Seismic velocity data indicate that the outer core does not transmit S-waves [2–4]. This observation and the lower density are interpreted to mean that the outer core is in a liquid state. The inner core transmits S-waves at very low velocities, suggesting it is a solid near the melting point or partly molten. The density deficit in the outer core is too large to be explained simply by a solid-liquid phase transition and it requires about 5-10 wt% (weight percent) of lower atomic weight elements to reduce its density and melting point [5, 6]. Reasonable estimates of the abundance and distribution of “light” elements in the core are essential to understanding the formation and evolution of the Earth, as well as how the core and mantle interact in the region around the core-mantle boundary (CMB) [7, 8].

Since F. Birch [5] suggested that pure Fe or Fe-Ni alloy alone is too dense, several light elements have been proposed as candidates existing in the Earth’s core, including O, Si, S, C, and H; ascertaining their varieties and concentrations has been a longstanding challenge. While the density distribution can be obtained from seismological remote sensing, the compositional structure of the Earth [9, 10] has been much more challenging to determine. Thus, the lower mantle and the core compositions remain uncertain despite significant advances in recent years. The estimates compare the density and sound velocity data from seismological observations with those from laboratory experiments and theoretical calculations [11]. It is difficult to conduct experiments with samples of liquid iron alloy under the extreme temperature and pressure conditions of the core [12] and, as a consequence, the available accurate experimental data are insufficient to be compared with seismological data directly. In recent work, the chemical composition of liquid iron alloys at outer-core pressure and temperature conditions has been constrained by comparing first principle calculations of the density and bulk sound velocity with the profiles of the Preliminary Reference Earth Model (PREM) [13]. The primary light component was found to be hydrogen when the inner-core boundary temperature T_{ICB} is not high (4800 K to 5400 K) or oxygen if $T_{\text{ICB}} = 6000$ K. Hence, as the authors conclude, it is still difficult to specify the outer-core chemical composition based solely on comparing theoretical calculations and seismological observations of the density and speed of sound.

Neutrino oscillation tomography is a new experimental technique that can provide complementary and independent information on the Earth’s internal structure [14]. The basic phenomenon is the modifications induced by terrestrial matter in the flavor transformations of low-energy atmospheric neutrinos (MeV to GeV) when passing through different regions of the planet. After decades of experimental observations and theoretical developments, the 3ν -oscillation paradigm has been firmly established as the mechanism underlying neutrino flavor transitions. In a medium, due to coherent forward scattering with background particles, the probabilities of the flavor transformations depend not only on the neutrino energy and the traveled distance z , but also on the electron number density $n_e(z)$ along the neutrino path [15, 16]:

$$n_e(z) = \frac{Z}{A}(z) \frac{\rho(z)}{m_{\text{u}}}, \quad (1)$$

where ρ is the matter density, $m_{\text{u}} = 931.494$ MeV is the atomic mass unit, and Z/A is the average

ratio between the atomic number Z and the (relative) atomic mass A . For a compound $Z(z)/A(z) = \sum_{\lambda} \mathbf{r}_{\lambda}(z) Z_{\lambda}/A_{\lambda}$, where the summation runs over all the elements contributing a fraction \mathbf{r}_{λ} to the total mass. Therefore, it might be possible to limit the permissible values of the density and composition of deep parts of the Earth by studying how changes in these quantities affect the number of events produced in a detector by neutrinos after they pass through the Earth [14, 17–27]. Except for hydrogen ($(Z/A)_H = 1$), all other light elements have nearly equal protons and neutrons and hence $Z/A \cong 0.5$ for them. Consequently, a small amount of hydrogen would cause a noticeable change in n_e , and neutrino oscillations could provide valuable information about the presence of this element in the core.

Out of the six neutrino oscillation parameters, Δm_{21}^2 , $|\Delta m_{31}^2|$, with $\Delta m_{ij}^2 = m_i^2 - m_j^2$, and the mixing angles $\theta_{12}, \theta_{13}, \theta_{23}$ of the matrix PMNS are known with ever-increasing accuracy [28]. The sign of Δm_{31}^2 characterizes the normal ordering (NO), with $m_3 > m_1$, and the inverted ordering (IO), with $m_3 < m_1$. Several experiments are already ongoing or in preparation to determine the neutrino mass ordering and the other two remaining issues: the value of the CP-violating phase δ and the octant of θ_{23} [29]. At the same time, these experiments will be sensitive to sub-leading effects associated with unknown interactions of neutrinos with ordinary matter parameterized at low energies by effective four-fermion couplings. They are generally referred to as non-standard neutrino interactions (NSI) (for reviews, see [30–32]) and can affect neutrino oscillation signals either through charged current (CC) processes, affecting neutrino production and detection, or through neutral current (NC) processes affecting neutrino propagation in matter. Such extensions of the standard framework have attracted the community’s attention because of the impact the additional interactions may have on getting the values of the oscillation parameters [33, 34]. Also, flavor-changing NC-NSI have been considered as a possible solution to the tension between the latest measurements of the CP phase from the long-baseline accelerator experiments NOvA and T2K [35].

In this work, we consider the application of atmospheric neutrino oscillations to examine the Earth’s internal composition, including possible effects due to NSI. Atmospheric neutrinos are produced isotropically in the upper atmosphere as decay products in hadronic showers generated in cosmic ray (usually protons) collisions with air nuclei. This provides a continuous source of neutrinos with travel distances from 15 to 12757 km to the detector and a wide range of energies, including the 1-10 GeV interval where the effects of terrestrial matter on the oscillations are significant. These characteristics make them well-suited for tomographic studies of the Earth’s interior. In concrete, we want to see to what extent NC-NSI effects on neutrino oscillations could affect the determination of the H content in the outer core and, vice versa, how compositional uncertainties could mask the effects associated with non-standard neutrino interactions. To this end, we analyze the ability of a large detector such as ORCA to resolve deviations in the number of μ -like events due to changes in the flavor content in the atmospheric neutrino flux as a consequence of modifications that a combination of the above-mentioned effects can have in neutrino oscillations in matter.

The paper is organized as follows. In section 2, we briefly review matter neutrino oscillations and describe the calculation of the transition probabilities, including NSI effects, for atmospheric neutrinos passing through the Earth, modeled as a sphere divided into 55 concentric shells integrated into five main layers. In section 3, we carry out a Monte Carlo simulation of the number of μ -like events in a detector like ORCA. The results and final comments are presented in section 4, where we

use our calculations to constrain the intensity of the non-standard interactions and the hydrogen content in the outer core.

2 Oscillations of atmospheric neutrinos

Neutrino dispersion relations are modified in a medium due to their coherent forward scattering with the background particles, in the normal matter: electrons (e), quarks up (u) y down (d). The scattering of ν_e with electrons differs from that of $\nu_{\mu,\tau}$ and, after subtracting an unobservable overall phase, this introduces an additional term in the Hamiltonian $H(z)$ that governs the evolution of the flavor amplitudes along the neutrino trajectory in matter. As a result, the pattern of neutrino oscillations can change in a non-trivial manner compared to vacuum oscillations, and resonance enhancement effects can appear under appropriate conditions.

Nonstandard neutral-current (NC) interactions may contribute to forward scattering processes and affect neutrino flavor transformations in the medium. At low energies, this can be conveniently studied within the frame of effective field theories parametrized in terms of four-fermion operators [15]. The NC-NSI effective Lagrangian at the quark level reads,

$$\mathcal{L}_{NSI} = -2\sqrt{2}G_F \sum_{f,\alpha,\beta} \epsilon_{\alpha\beta}^f (\bar{\nu}_\alpha \gamma^\mu P_L \nu_\beta) (\bar{f} \gamma^\mu f), \quad (2)$$

where G_F is the Fermi constant, $P_L = \frac{1}{2}(1 - \gamma_5)$, and the sum runs over the neutrino flavors ($\alpha, \beta = e, \mu, \tau$) and the charged fermions ($f = e, u, d$). We have assumed that the neutrino flavor structure of the interactions is independent of the charged fermion type [36]. The dimensionless coefficients $\epsilon_{\alpha\beta}^f$ quantify the strength of the NSI compared to the SM interactions: $\epsilon_{\alpha\beta}^f \sim O(G_X/G_W)$. Hermiticity of \mathcal{L}_{NSI} implies these coefficients satisfy $\epsilon_{\beta\alpha}^f = \epsilon_{\alpha\beta}^{f*}$ and hence, those with $\alpha = \beta$ are real.

For neutrinos propagating in ordinary matter, the contributions of the NC-NSI to the effective potential in the flavor evolution equation are:

$$\sqrt{2}G_F \sum_f n_f(z) \epsilon_{\alpha\beta}^f = \mathcal{V}(z) \left[\epsilon_{\alpha\beta} + \left(\frac{n_n(z)}{n_p(z)} - 1 \right) \epsilon_{\alpha\beta}^n \right], \quad (3)$$

where $\epsilon_{\alpha\beta} \equiv \epsilon_{\alpha\beta}^e + \epsilon_{\alpha\beta}^p + \epsilon_{\alpha\beta}^n$, $n_{p,n}(z)$ are the number densities of protons and neutrons, and $\mathcal{V}(z) = \sqrt{2}G_F n_e(z)$, with $n_e(z)$ the electron number density given in Eq. (1). When writing the right-hand side of the previous equation, we used the relations $n_u = 2n_p + n_n$ and $n_d = n_p + 2n_n$, and made the identifications $\epsilon_{\alpha\beta}^p = 2\epsilon_{\alpha\beta}^u + \epsilon_{\alpha\beta}^d$ and $\epsilon_{\alpha\beta}^n = 2\epsilon_{\alpha\beta}^d + \epsilon_{\alpha\beta}^u$. We also considered that, due to the neutrality of matter, $n_e(z) = n_p(z)$.

For Earth, the values of n_n/n_p given by the PREM are 1.012 in the mantle and 1.137 in the core. Therefore, assuming that the coefficients $\epsilon_{\alpha\beta}$ and $\epsilon_{\alpha\beta}^n$ have similar magnitudes, the second term in Eq. (3) is about ten times smaller than the first, and we will ignore it to keep our analysis as simple as possible. Thus, the Hamiltonian governing the evolution of the flavor amplitudes of atmospheric neutrinos traveling within terrestrial matter, in the basis of mass eigenstates, is given by:

$$H(z) = \begin{pmatrix} 0 & 0 & 0 \\ 0 & \Delta_{21} & 0 \\ 0 & 0 & \Delta_{31} \end{pmatrix} + \mathcal{V}(z) U^\dagger \begin{pmatrix} 1 + \epsilon_{ee} - \epsilon_{\mu\mu} & \epsilon_{e\mu} & \epsilon_{e\tau} \\ \epsilon_{\mu e} & 0 & \epsilon_{\mu\tau} \\ \epsilon_{\tau e} & \epsilon_{\tau\mu} & \epsilon_{\tau\tau} - \epsilon_{\mu\mu} \end{pmatrix} U, \quad (4)$$

where U is the PMNS mixing matrix and the “one” in the ee entry of the effective potential matrix accounts for the standard charged-current contribution. In writing $H(z)$, the usual non-relativistic approximation $E_i - E_j \cong \Delta_{ij}$ was used and the $\mu\mu$ element of the potential energy matrix was subtracted by factoring a global phase proportional to $\epsilon_{\mu\mu}$. The probabilities $P_{\nu_\alpha \rightarrow \nu_\beta}(z)$ that a

Parameter	Normal Ordering	Inverted Ordering
Δm_{21}^2 [eV ²]	7.42×10^{-5}	7.42×10^{-5}
Δm_{31}^2 [eV ²]	2.533×10^{-3}	-2.437×10^{-3}
$\sin^2 \theta_{12}$	0.309	0.308
$\sin^2 \theta_{13}$	0.0223	0.0232
$\sin^2 \theta_{23}$	0.561	0.564
δ/π	1.19	1.54

Table 1: Three-neutrino oscillation parameters obtained by averaging the best-fit values of three recent global fits of the current neutrino oscillation data [37–39].

neutrino produced as a ν_α is found in a flavor ν_β at a distance z from the source can be written as:

$$P_{\nu_\alpha \rightarrow \nu_\beta}(z) = |\mathcal{U}_{\beta\alpha}(z)|^2, \quad (5)$$

where $\mathcal{U}_{\beta\alpha}(z) = \langle \nu_\beta | \hat{U}(z) | \nu_\alpha \rangle$ are the elements of the 3×3 matrix $\mathcal{U}_f(z)$ representing the evolution operator in the flavor basis. This matrix is related to that in the mass eigenstates basis, $\mathcal{U}_m(z)$, by the unitary transformation

$$\mathcal{U}_f(z) = U \mathcal{U}_m(z) U^\dagger, \quad (6)$$

where \mathcal{U}_m has to be determined by solving the equation

$$i \frac{d}{dz} \mathcal{U}_m(z) = H(z) \mathcal{U}_m(z), \quad \mathcal{U}_m(0) = I, \quad (7)$$

with $H(z)$ given by the matrix in Eq. (4).

In the present study, we use a spherically symmetric one-dimensional model of our home planet consisting of 55 concentric shells, each with a constant density equal to the average value of the PREM densities in the shell. The set of shells is divided into five main layers bounded by concentric spheres of different radii: inner core (*IC*), outer core (*OC*), lower mantle (M_1), upper mantle (M_2), and crust (*C*). The compositions and radii of these layers are given in Table 2. We take the same Z/A for the entire mantle and the same for the inner and outer core. The values of the radii are those of the PREM. We will refer to this model as the *standard Earth*. To appreciate the effect of changes in composition, we will compare it with models that contain some percentage of hydrogen in the outer core.

The complete evolution operator can be expressed as the product of the evolution operators of the consecutive shells through which the neutrinos pass on their way to the detector:

$$\mathcal{U}_m(L) = \prod_{j=1}^{2j_m-1} \mathcal{U}_m^j(L_j), \quad (8)$$

by applying the Cayley-Hamilton theorem, which allows us to convert the infinity series into a polynomial:

$$\mathcal{U}_m^j(L_j) = a_0^j I + a_1^j H_j + a_2^j H_j^2, \quad (12)$$

where the coefficients are functions of the eigenvalues of H_j [24, 40].

The relevant quantities for us are the oscillation probabilities for $\nu_\mu(\bar{\nu}_\mu) \rightarrow \nu_{\mu,\tau}(\bar{\nu}_{\mu,\tau})$ and $\nu_e(\bar{\nu}_e) \rightarrow \nu_{\mu,\tau}(\bar{\nu}_{\mu,\tau})$, which are needed to compute the μ -like events produced in a detector by “upward” atmospheric neutrinos after traveling a distance L through the Earth. Due to the dependence of these probabilities on the potential $V(z)$, they are sensitive to changes in the density and composition of the traversed internal regions of the Earth. In what follows, we look into the feasibility of applying such an effect to obtain meaningful information about the hydrogen content in the outer core using atmospheric neutrino oscillations in the presence of NSI.

3 Neutrino events and test of Earth’s composition with NSI

Let us consider a generic detector with a water or ice mass containing n_N nucleons as a target, which can efficiently detect Cherenkov radiation emitted along the trajectories of the μ^\pm produced by the interactions of ν_μ and $\bar{\nu}_\mu$ with nucleons in or near the instrumented volume. It can also detect neutrino showers due to the e or τ produced by the associated neutrinos [23, 41, 42]. To generate a data set that resembles real observations, with the inevitable statistical fluctuations, we performed a Monte Carlo simulation of the neutrino events, employing the same procedure implemented in [24], which we summarize below.

Our observable is the number \mathcal{N}_μ of μ -like events within given angular and energy intervals:

$$\begin{aligned} \mathcal{N}_\mu = n_N T \int_{E_{\min}}^{E_{\max}} dE \int_{\eta_{\min}}^{\eta_{\max}} d\Omega & \left[\sigma_{\nu_\mu}^{cc}(E) \left(P_{\nu_\mu \rightarrow \nu_\mu} \frac{d\Phi^{\nu_\mu}}{dE} + P_{\nu_e \rightarrow \nu_\mu} \frac{d\Phi^{\nu_e}}{dE} \right) + \right. \\ & \sigma_{\bar{\nu}_\mu}^{cc}(E) \left(P_{\bar{\nu}_\mu \rightarrow \bar{\nu}_\mu} \frac{d\Phi^{\bar{\nu}_\mu}}{dE} + P_{\bar{\nu}_e \rightarrow \bar{\nu}_\mu} \frac{d\Phi^{\bar{\nu}_e}}{dE} \right) + \\ & \sigma_{\nu_\tau}^{cc}(E) Br_{\tau \rightarrow \mu} \left(P_{\nu_\mu \rightarrow \nu_\tau} \frac{d\Phi^{\nu_\mu}}{dE} + P_{\nu_e \rightarrow \nu_\tau} \frac{d\Phi^{\nu_e}}{dE} \right) + \\ & \left. \sigma_{\bar{\nu}_\tau}^{cc}(E) Br_{\bar{\tau} \rightarrow \bar{\mu}} \left(P_{\bar{\nu}_\mu \rightarrow \bar{\nu}_\tau} \frac{d\Phi^{\bar{\nu}_\mu}}{dE} + P_{\bar{\nu}_e \rightarrow \bar{\nu}_\tau} \frac{d\Phi^{\bar{\nu}_e}}{dE} \right) \right], \quad (13) \end{aligned}$$

where T is the detection time and $Br_{\tau \rightarrow \mu} = Br_{\bar{\tau} \rightarrow \bar{\mu}} \simeq 0.17$ are the branching ratios of the decays $\tau \rightarrow \mu \bar{\nu}_\mu \nu_\tau$ and $\bar{\tau} \rightarrow \bar{\mu} \nu_\mu \bar{\nu}_\tau$. The fluxes of atmospheric neutrinos and antineutrinos were taken from Ref. [43]. The dependence of \mathcal{N}_μ on the density and composition of the medium is incorporated through the neutrino oscillation probabilities, calculated with the expressions in Sec. 2 evaluated at a distance L . The values of the oscillation parameters are those given in Table 1 and correspond to the mean of the best-fit values for the allowed ranges at 1σ of the global analyses performed by three groups [37–39].

As shown in Ref. [24], the region where \mathcal{N}_μ is most sensitive to changes in the outer core compositions lies in the intervals $4 \text{ GeV} < E < 10 \text{ GeV}$ and $10^\circ < \eta < 60^\circ$ of the neutrinos’s energy and nadir angle, respectively. The charged-current cross sections for the $\nu_\mu(\bar{\nu}_\mu)$ - nucleon and

$\nu_\tau(\bar{\nu}_\tau)$ -nucleon scatterings, in this energy range are given approximately by [44]:

$$\begin{aligned}
\sigma_{\nu_\mu}^{cc}(E) &\simeq 0.75 \times 10^{-38} (E/\text{GeV}) \text{ cm}^2, \\
\sigma_{\bar{\nu}_\mu}^{cc}(E) &\simeq 0.35 \times 10^{-38} (E/\text{GeV}) \text{ cm}^2, \\
\sigma_{\nu_\tau}^{cc}(E) &\simeq 0.13 \times 10^{-38} (E/\text{GeV}) \text{ cm}^2, \\
\sigma_{\bar{\nu}_\tau}^{cc}(E) &\simeq 0.05 \times 10^{-38} (E/\text{GeV}) \text{ cm}^2.
\end{aligned}
\tag{14}$$

NSI also affect neutrino production and detection through charged-current interactions (CC). In general, the limits for CC-NSI are an order of magnitude more restrictive than for NC-NSI [45–47], and in this work, we disregard their effects on detection.

The region delimited by the energy and angle intervals indicated above is divided into 200×200 square bins. Every pseudo experiment is made up by tossing in each bin (i, j) of the grid, several Poisson distributed events with the mean value equal to \mathcal{N}_μ as given by Eq. (13). Thus, each of the n_{exp} experiments consists of 200×200 numbers corresponding to events, one for each bin. These are called the *true events* and assumed to be distributed according to the probability distribution function (pdf) $f_t^{i_{exp}}(E, \eta)$, $i_{exp} = 1, \dots, n_{exp}$, given by the normalized histograms constructed using the Monte Carlo simulation. A realistic distribution of events is implemented by folding the true distribution with the resolution function

$$\mathcal{S}(E_o, \eta_o | E, \eta) = \frac{1}{2\pi\Delta\eta(E)\Delta E(E)} \exp\left(-\frac{(\eta - \eta_o)^2}{2\Delta\eta(E)^2}\right) \exp\left(-\frac{(E - E_o)^2}{2\Delta E(E)^2}\right),
\tag{15}$$

with the detector characterized by the angular and energy resolutions $\Delta\eta(E) = \alpha_\eta/\sqrt{E/\text{GeV}}$ and $\Delta E(E) = \alpha_E E$, respectively. For the values of the parameters α_η and α_E , different situations are possible, as discussed in Ref. [21]. To keep our analysis as simple as possible, we assume a detection efficiency of 100%. In terms of the resolution function, the number of *observed events* $\mathcal{O}_{m,n}^{i_{exp}}$ in the bin (m, n) for the i_{exp} -th experiment is given by:

$$\mathcal{O}_{m,n}^{i_{exp}} = \mathcal{N}_{tot} \sum_{i,j} \iint_{\text{bin}(m,n)} dE_o d\eta_o \iint_{\text{bin}(i,j)} dE d\eta \mathcal{S}(E_o, \eta_o | E, \eta) f_t^{i_{exp}}(E, \eta).
\tag{16}$$

As an illustration, in Figs. 2 and 3 we show the pdf of the observed and true events as functions of the energy and nadir angle, for NO and IO, respectively, in the case of the standard Earth defined above, as it was shown in [48]. The figures were made using the same (large) number of bins for both kinds of events, but these numbers generally differ. In what follows, to test how well the hypothesis of different Earth compositions is in agreement with the standard Earth, we take the observed events to be distributed into five angular bins and nine energy bins. From Eq. (16), for each bin (m, n) , with $m = 1, \dots, 9$ and $n = 1, \dots, 5$, we determine the number of events $\mathcal{O}_\alpha^{0 i_{exp}}$ for the standard Earth and $\mathcal{O}_\alpha^{i_{exp}}(\text{H}, \epsilon)$ for an alternative Earth with different H content in the outer core and non-null NSI interactions generically labeled by ϵ . Here, $\alpha = 1, \dots, 45$ label the two-dimensional bins (m, n) . Thus, for each of these bins, we have a sample of the observed events and determine the corresponding

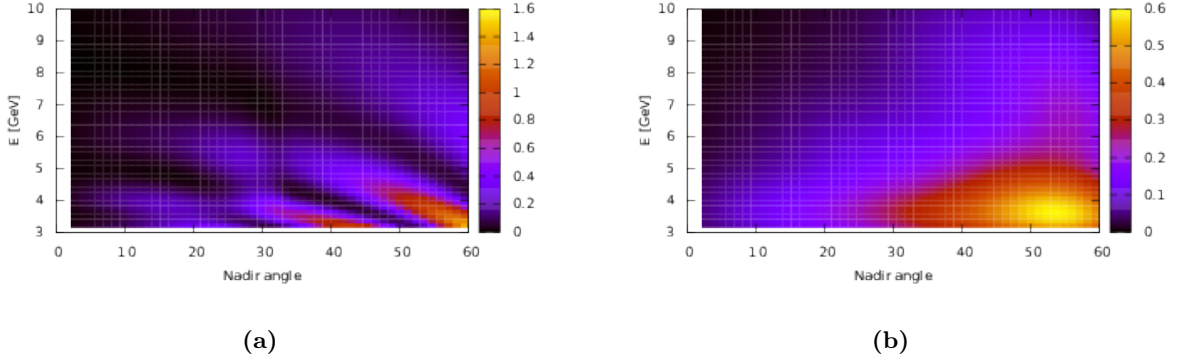


Figure 2: Probability distribution for (a) true and (b) observed events, for normal mass ordering.

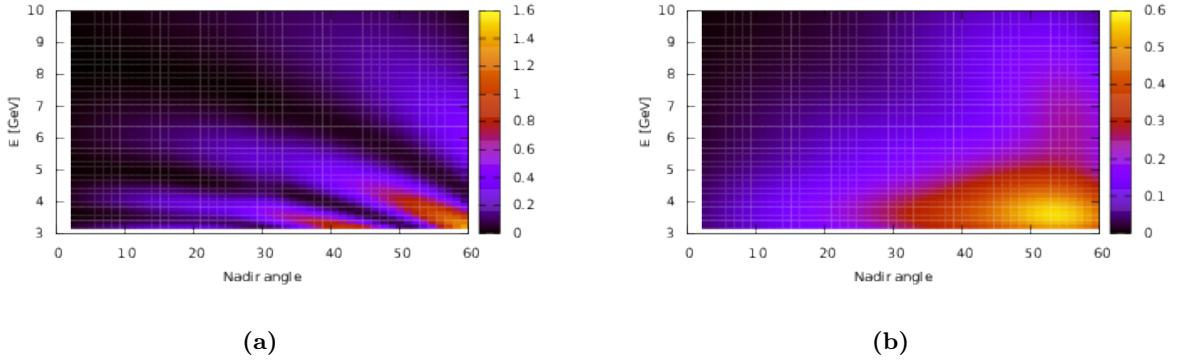


Figure 3: Probability distribution for (a) true and (b) observed events, for inverted mass ordering.

mean values

$$\begin{aligned}\bar{\mathcal{O}}_\alpha^0 &= \frac{1}{n_{exp}} \sum_{i_{exp}} \mathcal{O}_\alpha^{0 i_{exp}}, \\ \bar{\mathcal{O}}_\alpha(\mathbb{H}, \epsilon) &= \frac{1}{n_{exp}} \sum_{i_{exp}} \mathcal{O}_\alpha^{i_{exp}(\mathbb{H}, \epsilon)}.\end{aligned}\quad (17)$$

For Poisson distributed events, in terms of the likelihood function L , we construct the negative log-likelihood ratio function as

$$\chi_\lambda^2 = -\ln \left[\frac{L(\bar{\mathcal{O}}_\alpha^0; \bar{\mathcal{O}}_\alpha(\mathbb{H}, \epsilon))}{L(\bar{\mathcal{O}}_\alpha^0, \bar{\mathcal{O}}_\alpha^0)} \right] = 2 \sum_\alpha \left[\bar{\mathcal{O}}_\alpha(\mathbb{H}, \epsilon) - \bar{\mathcal{O}}_\alpha^0 \ln \left(\frac{\bar{\mathcal{O}}_\alpha^0}{\bar{\mathcal{O}}_\alpha(\mathbb{H}, \epsilon)} \right) \right]. \quad (18)$$

According to Wilks' theorem [49] the χ_λ^2 distribution can be approximated by the χ^2 distribution and, from it, the goodness of the fit can be established. The statistical significance of the χ^2 test is given, as usual, by the **p**-value:

$$\mathbf{p} = \int_{\chi^2}^{\infty} f_\chi(w, n_{\text{dof}}) dw, \quad (19)$$

where n_{dof} is the number of degrees of freedom and $f_\chi(w, n_{\text{dof}})$ is the chi-square distribution. In our case, $n_{\text{dof}} = 9 \times 5 - 2 = 43$. Thus, we can examine the levels of a discrepancy between the standard

Earth and different hypotheses about the composition of the outer core. This is done in the next section, with attention paid to how this can be affected by new physics effects in the neutrino sector.

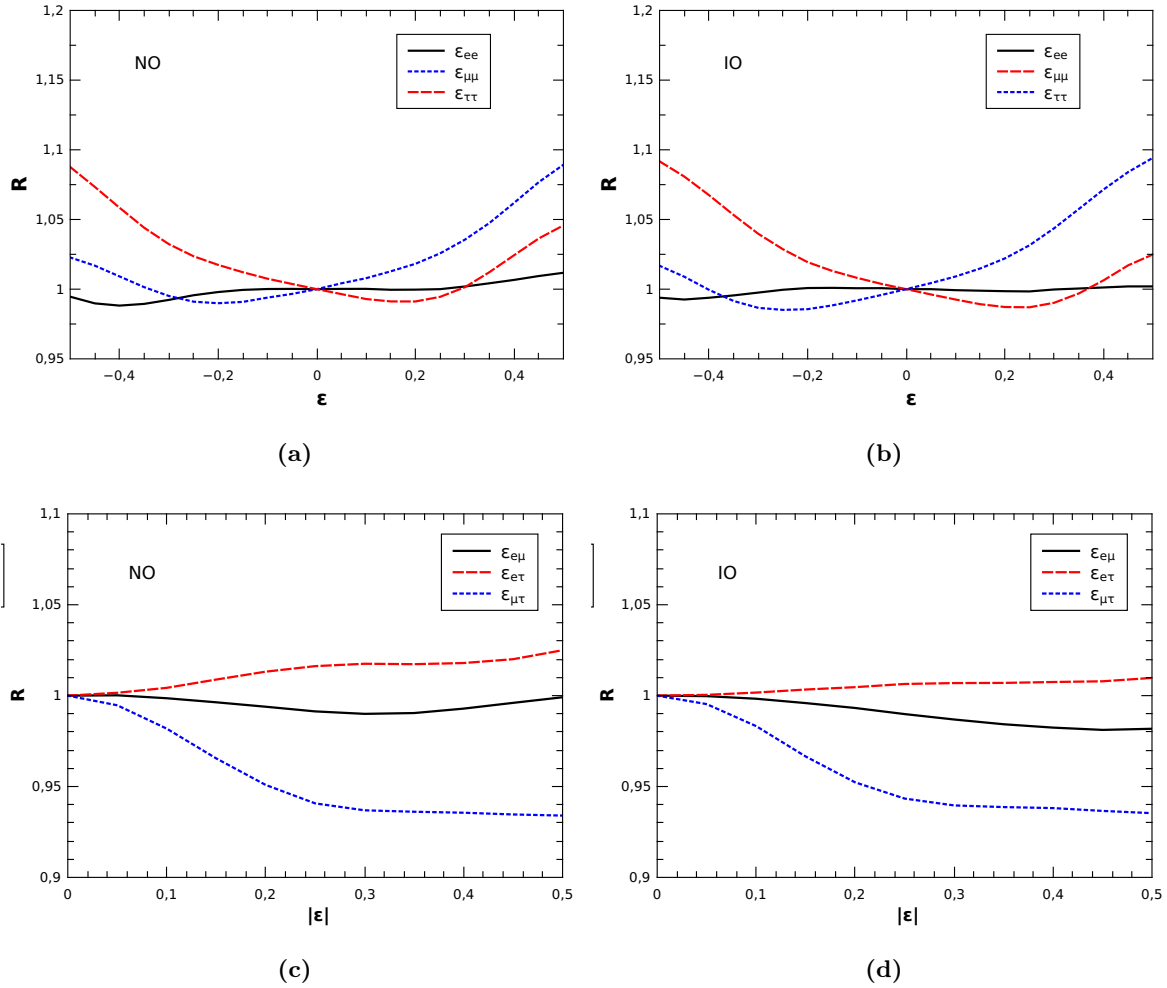


Figure 4: $R(\epsilon) = \mathcal{N}_\mu(\epsilon)/\mathcal{N}_\mu(0)$ as a function of a single non-null parameter of the matrix $(\epsilon_{\alpha\beta})$, for the standard Earth and normal and inverted ordering. (a, b) Diagonal coefficients $\epsilon_{ee}, \epsilon_{\mu\mu}, \epsilon_{\tau\tau}$; (c, d) Non-diagonal coefficients $\epsilon_{e\mu}, \epsilon_{e\tau}, \epsilon_{\mu\tau}$.

4 Results and Final Comments

Our goal is to see to what extent the presence of hydrogen in the outer core can be detected through the modifications it introduces in the flavor transformations of atmospheric neutrinos when NSI effects are included. To visualize the behavior of the events as a function of the coefficients $\epsilon_{\alpha\beta}$ we introduce the quantity

$$R(\epsilon) \equiv \frac{\mathcal{N}_\mu(\epsilon)}{\mathcal{N}_\mu(0)}, \quad (20)$$

which gives the relative size between the number $\mathcal{N}_\mu(\epsilon)$ of μ events in the energy and angle intervals considered, calculated including the effect of different NC-NSI entries of the potential energy matrix,

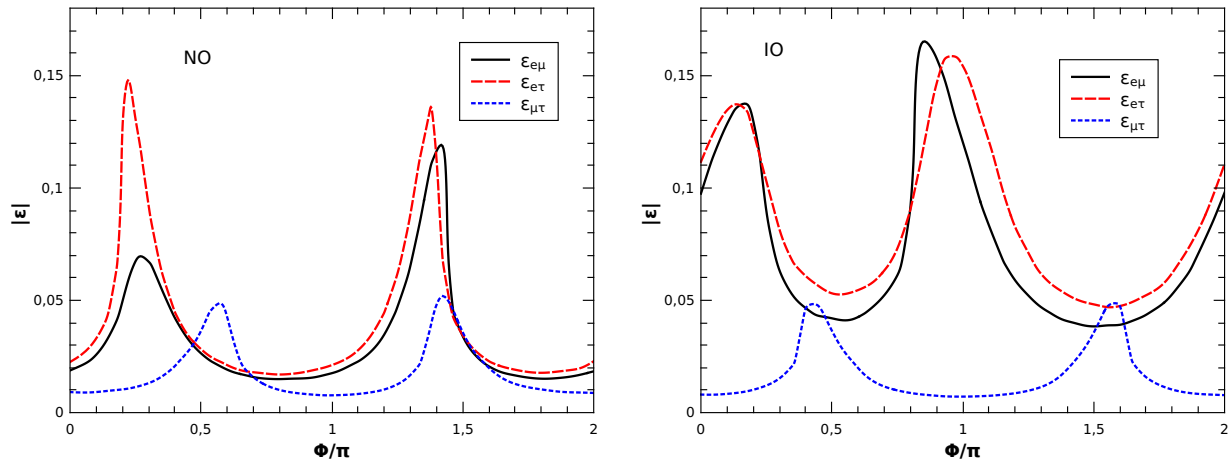


Figure 5: Bounds on the modulus and phase of the non-diagonal entries of the matrix $(\epsilon_{\alpha\beta})$, for (a) normal ordering and (b) inverted ordering. The allowed values fall in the regions under the curves, where the discrepancy between the events with and without the NSI is less than 1σ .

and the number $\mathcal{N}_\mu(0)$ calculated for standard interactions only. In Fig. 4, we show $R(\epsilon)$ as a function of different $\epsilon_{\alpha\beta}$ ($\alpha, \beta = e, \mu, \tau$) of the effective neutrino potential matrix, for the standard Earth, and normal ordering (NO) and inverted ordering (IO).

The quantities to be adjusted are the proportion of H in the outer core and the magnitudes of the different entries $\epsilon_{\alpha\beta}$ of the effective neutrino potential matrix. To take a first look at the allowed values of these coefficients, for the non-diagonal entries we construct regions in the plane $(\epsilon_{\alpha\beta}, \arg(\epsilon_{\alpha\beta}/\pi))$, $\alpha \neq \beta$. This is done for the standard Earth and the oscillation parameters given in Table 1, assuming an operation during 10 years of an 8 Mton detector like ORCA, with resolution parameters $\alpha_\eta = 0.25$ and $\alpha_E = 0.2$. In Fig. 5, we show the limits for the moduli and phase of the complex functions $\epsilon_{e\tau}, \epsilon_{e\mu}, \epsilon_{\mu\tau}$, for NO and IO. The allowed values lie in the regions under the curves, where the statistical significance of the discrepancy between the events with and without the NSI is less than a significance level of 1σ for one d.o.f. These values are compatible with the bounds reported in the literature [34]. Next, to show how the presence of NSI can affect the tomographic studies of the outer core composition $(Z/A)_{oc}$, utilizing the same procedure outlined in the previous paragraph, we construct regions in the plane $((Z/A)_{oc}, \epsilon_{\alpha\beta})$. In Figs. 6a and 6b we present the graphs for the real diagonal entries $\epsilon_{ee} - \epsilon_{\mu\mu}$ and $\epsilon_{\tau\tau} - \epsilon_{\mu\mu}$ versus the outer core composition, while in Figs. 6c and 6d we show the corresponding graphs for the modules of the complex off-diagonal entries $\epsilon_{e\mu}, \epsilon_{e\tau}, \epsilon_{\mu\tau}$, with the respective phases marginalized. The allowed values lie in the regions inside the curves, where again, the statistical significance of the difference between events with and without NSI on the Earth with and without H is less than a significance level of 1σ for one d.o.f. As can be seen, the regions for NO are considerably more restrictive than those for IO. The regions to the right of the vertical dashed line correspond to the standard composition plus the addition of hydrogen in the outer core. Assuming that the variation in the composition of the outer core is associated exclusively with the abundance of hydrogen, we have

$$(Z/A)_{oc} = (1 - F_H)(Z/A)_{oc}^0 + F_H(Z/A)_{oc}^H, \quad (21)$$

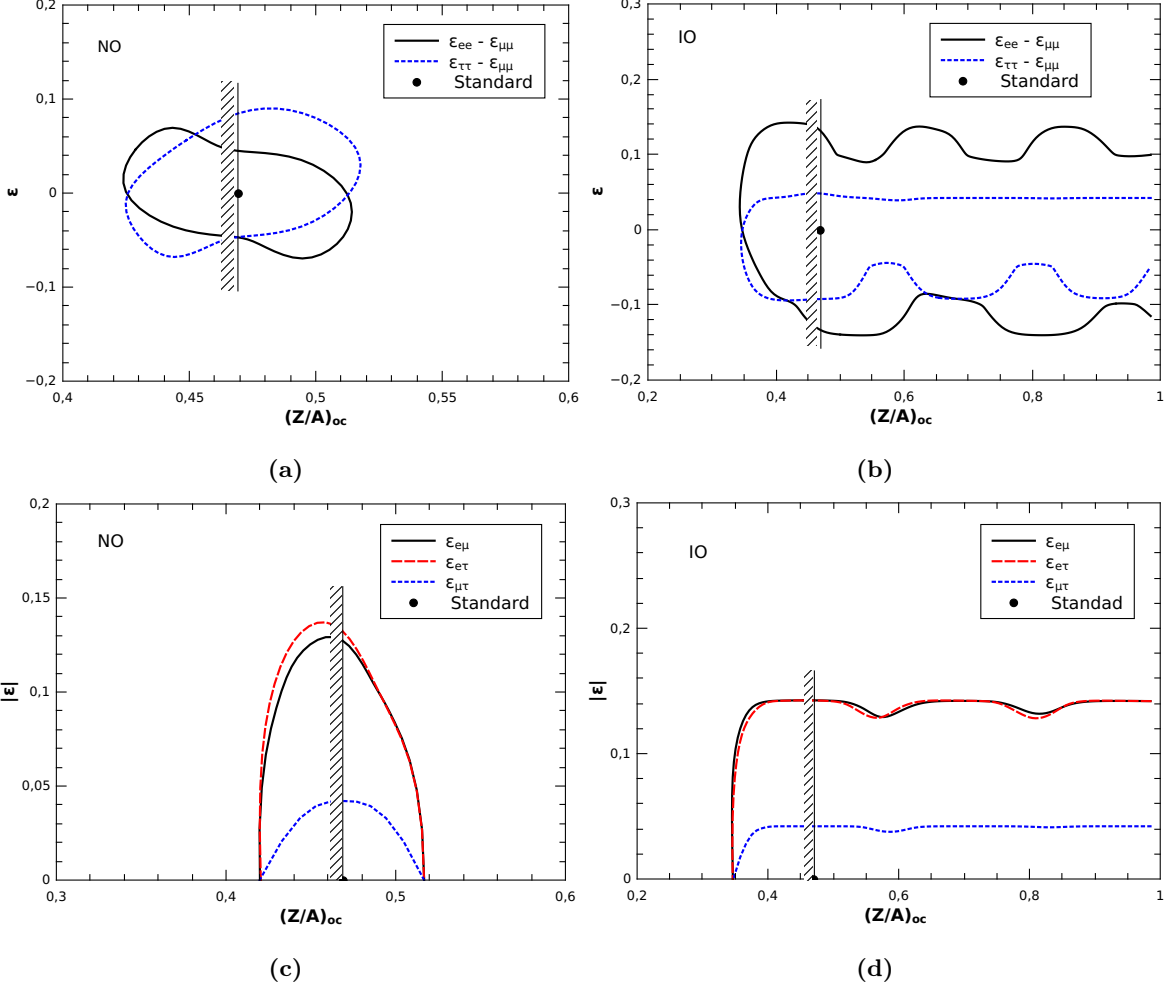


Figure 6: A single non-null entry of the matrix $(\epsilon_{\alpha\beta})$ as a function of the outer core composition. (a, b) Diagonal coefficients $\epsilon_{ee} - \epsilon_{\mu\mu}$, $\epsilon_{\tau\tau} - \epsilon_{\mu\mu}$; (c, d) Non-diagonal coefficients $\epsilon_{e\mu}$, $\epsilon_{e\tau}$, $\epsilon_{\mu\tau}$, with the respective phase marginalized. The regions enclosed by the contours correspond to the expected 1σ statistical significance of the difference between events with and without NSI on the Earth with and without H in the outer core, for normal and inverted ordering. The regions to the right of the vertical dashed line correspond to the standard composition plus the addition of hydrogen in the outer core.

where $(Z/A)_{oc}^0 = 0.4691$ is the value with no hydrogen and $F_H = M_H/M_{oc}$ is the fractional contribution that hydrogen makes to the total mass of the layer.

In summary, the next generation of neutrino detectors could efficiently detect the presence of a small percentage of hydrogen in the outer core by means of neutrino oscillation tomography of the Earth. This will also have the potential to investigate physics beyond the Standard Model, usually described in a model-independent manner by NSI. In this work, we consider the combined effects of uncertainties in the composition of deep Earth regions and NSI on the propagation of atmospheric neutrinos within terrestrial matter. Our goal was to examine the interplay between these two effects: to what extent NSI can hinder the acquisition of compositional information and, vice versa, how compositional uncertainties could mask new physics effects. Using as physical observables the μ -type

events produced in a generic large Cherenkov detector and doing a Monte Carlo simulation of the energy and azimuthal angle distribution of these events, we test possible variations in the composition of the outer core together with the effects of new interactions in the neutrino sector. Considering neutrino oscillations in a standard Earth, without H in the core, we constrain the possible values of the dimensionless coefficients $\epsilon_{\alpha\beta}$ that parametrize the NSI intensities relative to the SM interactions. Then, for the normal-ordering and inverted-ordering neutrino masses, we determined the correlated 1σ limits on the outer core composition and the diagonal and non-diagonal NSI coefficients. In the non-diagonal case, the phase of the complex coefficient was marginalized. The corresponding plots are presented in Fig. 6, where the regions to the right of the vertical dashed line correspond to the standard composition modified by the addition of hydrogen. The limits on the composition change due to modifications of the flavor probability transitions caused by NSI. This is particularly evident in Fig. 6a, where it is observed a positive (negative) correlation between $\epsilon_{\tau\tau} - \epsilon_{\mu\mu}$ ($\epsilon_{ee} - \epsilon_{\mu\mu}$) and $(Z/A)_{oc}$. In particular, it is possible to observe the increase of the allowed values for $(Z/A)_{oc}$ in the case of no null values of ϵ . As an indication that our results are correct, we note that for $\epsilon = 0$ we recover the outer core composition range obtained considering only the standard interactions [48]. Since, as shown in Fig. 5, our bounds for the magnitude of the NSI coefficients are of the same order as those in the literature, one can infer that more restrictive limits on these coefficients could be needed to obtain confident values of the hydrogen content in the Earth's outer core through an oscillation tomographic search.

Acknowledgments

This work was supported by UNAM PASPA-DGAPA, CONAHCYT (Mexico) through grant CF-2023-I-1169, and the Consejo Nacional de Investigaciones Cientificas y Tecnicas (CONICET) and the UNMDP Mar del Plata, Argentina.

References

- [1] Clement, B., Holzheid, A. & Tilgner, A. Core geophysics. *Proceedings of the National Academy of Sciences of the United States of America* **94**, 12742–3 (1997). 2
- [2] Jeanloz, R. The Nature of the Earth’s Core. *Annual Review of Earth and Planetary Sciences* **18**, 357 (1990). 2
- [3] Jacobs, J. A. The earth’s core in a nutshell. *Nature* **356**, 286–287 (1992). URL <https://doi.org/10.1038/356286a0>. 2
- [4] Tkalčić, H. & Kennett, B. L. N. Core structure and heterogeneity: a seismological perspective. *Australian Journal of Earth Sciences* **55**, 419–431 (2008). URL <https://doi.org/10.1080/08120090801888578>. <https://doi.org/10.1080/08120090801888578>. 2
- [5] Birch, F. Density and composition of mantle and core. *Journal of Geophysical Research* **57**, 4377–4388 (1964). 2
- [6] Poirier, J.-P. Light elements in the earth’s outer core: A critical review. *Physics of the Earth and Planetary Interiors* **85**, 319–337 (1994). URL <https://www.sciencedirect.com/science/article/pii/0031920194901201>. 2
- [7] Litasov, K. & Shatskiy, A. Composition of the earth’s core: A review. *Russian Geology and Geophysics* **57**, 22–46 (2016). 2
- [8] Hirose, K., Wood, B. & Vočadlo, L. Light elements in the earth’s core. *Nature Reviews Earth & Environment* **2**, 645–658 (2021). URL <https://doi.org/10.1038/s43017-021-00203-6>. 2
- [9] Allègre, C. J., Poirier, J.-P., Humler, E. & Hofmann, A. W. The chemical composition of the earth **134**, 515–526. 2
- [10] McDonough, W. & Sun, S. The composition of the earth. *Chemical Geology* **120**, 223–253 (1995). URL <https://www.sciencedirect.com/science/article/pii/0009254194001404>. Chemical Evolution of the Mantle. 2
- [11] Zhang, Y. *et al.* Experimental constraints on light elements in the earth’s outer core **6**. 2
- [12] Morard, G. *et al.* The Earth’s core composition from high pressure density measurements of liquid iron alloys. *Earth and Planetary Science Letters* **373**, 169–178 (2013). 2
- [13] Umemoto, K. & Hirose, K. Chemical compositions of the outer core examined by first principles calculations. *Earth and Planetary Science Letters* **531**, 116009 (2020). URL <http://www.sciencedirect.com/science/article/pii/S0012821X19307010>. 2
- [14] Winter, W. Neutrino tomography: Learning about the earth’s interior using the propagation of neutrinos. *Earth Moon Planets* **99**, 285–307 (2006). [physics/0602049](https://doi.org/10.1007/s11067-006-9060-9). 2, 3
- [15] Wolfenstein, L. Neutrino oscillations in matter. *Phys. Rev. D* **17**, 2369–2374 (1978). URL <https://link.aps.org/doi/10.1103/PhysRevD.17.2369>. 2, 4

-
- [16] Mikheyev, S. P. & Smirnov, A. Y. Resonance amplification of oscillations in matter and spectroscopy of solar neutrinos. *Sov. J. Nucl. Phys.* **42**, 913–917 (1985). [2](#)
- [17] Nicolaidis, A. Neutrinos for Geophysics. *Phys. Lett. B* **200**, 553–559 (1988). [3](#)
- [18] Nicolaidis, A., Jannane, M. & Tarantola, A. Neutrino tomography of the earth. *J. Geophys. Res.* **96**, 21811–21817 (1991). [3](#)
- [19] Borriello, E. *et al.* Sensitivity on Earth Core and Mantle densities using Atmospheric Neutrinos. *JCAP* **06**, 030 (2009). [0904.0796](#). [3](#)
- [20] Winter, W. Atmospheric Neutrino Oscillations for Earth Tomography. *Nucl. Phys. B* **908**, 250–267 (2016). [1511.05154](#). [3](#)
- [21] Rott, C., Taketa, A. & Bose, D. Spectrometry of the Earth using Neutrino Oscillations. *Sci. Rep* **5**, 15225 (2015). [1502.04930](#). [3](#), [8](#)
- [22] Bourret, S., Coelho, J. A. & Van Elewyck, V. Neutrino oscillation tomography of the Earth with KM3NeT-ORCA. *PoS ICRC2017*, 1020 (2018). [3](#)
- [23] Bourret, S., Coelho, J. A. B., Elewyck, V. V. & on behalf of the KM3NeT collaboration. Neutrino oscillation tomography of the earth with km3net-orca. *Journal of Physics: Conference Series* **888**, 012114 (2017). URL <https://dx.doi.org/10.1088/1742-6596/888/1/012114>. [3](#), [7](#)
- [24] D’Olivo, J. C., Herrera Lara, J. A., Romero, I., Sampayo, O. A. & Zapata, G. Earth tomography with atmospheric neutrino oscillations. *Eur. Phys. J. C* **80**, 1001 (2020). [3](#), [7](#)
- [25] Kelly, K. J., Machado, P. A. N., Martinez-Soler, I. & Perez-Gonzalez, Y. F. Dune atmospheric neutrinos: Earth tomography. *Journal of High Energy Physics* **2022**, 187 (2022). URL [https://doi.org/10.1007/JHEP05\(2022\)187](https://doi.org/10.1007/JHEP05(2022)187). [3](#)
- [26] Upadhyay, A. K., Kumar, A., Agarwalla, S. K. & Dighe, A. Probing dark matter inside earth using atmospheric neutrino oscillations at ino-ical. *Phys. Rev. D* **107**, 115030 (2023). URL <https://link.aps.org/doi/10.1103/PhysRevD.107.115030>. [3](#)
- [27] Maderer, L., Kaminski, E., Coelho, J. A. B., Bourret, S. & Van Elewyck, V. Unveiling the outer core composition with neutrino oscillation tomography. *Front. Earth Sci.* **11**, 1008396 (2023). [2208.00532](#). [3](#)
- [28] Navas, S. *et al.* Review of particle physics. *Phys. Rev. D* **110**, 030001 (2024). URL <https://link.aps.org/doi/10.1103/PhysRevD.110.030001>. [3](#)
- [29] Jamieson, B. Future neutrino experiments (2022). URL <https://arxiv.org/abs/2207.05044>. [2207.05044](#). [3](#)
- [30] Ohlsson, T. Status of non-standard neutrino interactions. *Reports on Progress in Physics* **76**, 044201 (2013). URL <http://dx.doi.org/10.1088/0034-4885/76/4/044201>. [3](#)

-
- [31] Miranda, O. G. & Nunokawa, H. Non standard neutrino interactions: current status and future prospects. *New Journal of Physics* **17**, 095002 (2015). URL <https://dx.doi.org/10.1088/1367-2630/17/9/095002>. 3
- [32] Farzan, Y. & Tórtola, M. Neutrino oscillations and non-standard interactions. *Frontiers in Physics* **6**, 10 (2018). URL <https://www.frontiersin.org/journals/physics/articles/10.3389/fphy.2018.00010>. 1710.09360. 3
- [33] Capozzi, F., Chatterjee, S. S. & Palazzo, A. Neutrino Mass Ordering Obscured by Nonstandard Interactions. *Phys. Rev. Lett.* **124**, 111801 (2020). 1908.06992. 3
- [34] Esteban, I., Gonzalez-Garcia, M. C. & Maltoni, M. On the determination of leptonic cp violation and neutrino mass ordering in presence of non-standard interactions: present status. *Journal of High Energy Physics* **2019**, 55 (2019). URL [https://doi.org/10.1007/JHEP06\(2019\)055](https://doi.org/10.1007/JHEP06(2019)055). 1905.05203. 3, 11
- [35] Chatterjee, S. S. & Palazzo, A. Nonstandard Neutrino Interactions as a Solution to the $NO\nu A$ and T2K Discrepancy. *Phys. Rev. Lett.* **126**, 051802 (2021). 2008.04161. 3
- [36] Esteban, I., Gonzalez-Garcia, M. C., Maltoni, M., Martinez-Soler, I. & Salvado, J. Updated constraints on non-standard interactions from global analysis of oscillation data. *Journal of High Energy Physics* **2018**, 180 (2018). URL [https://doi.org/10.1007/JHEP08\(2018\)180](https://doi.org/10.1007/JHEP08(2018)180). 4
- [37] Capozzi, F. *et al.* Addendum to Global constraints on absolute neutrino masses and their ordering. *Phys. Rev. D* **101**, 116013 (2020). URL <https://link.aps.org/doi/10.1103/PhysRevD.101.116013>. 5, 7
- [38] Esteban, I., Gonzalez-Garcia, M. C., Maltoni, M., Schwetz, T. & Zhou, A. The fate of hints: updated global analysis of three-flavor neutrino oscillations. *Journal of High Energy Physics* **2020**, 178 (2020). URL [https://doi.org/10.1007/JHEP09\(2020\)178](https://doi.org/10.1007/JHEP09(2020)178). 5, 7
- [39] de Salas, P. F. *et al.* 2020 global reassessment of the neutrino oscillation picture. *Journal of High Energy Physics* **2021**, 71 (2021). URL [https://doi.org/10.1007/JHEP02\(2021\)071](https://doi.org/10.1007/JHEP02(2021)071). 5, 7
- [40] Ohlsson, T. & Snellman, H. Three flavor neutrino oscillations in matter. *J. Math. Phys.* **41**, 2768–2788 (2000). [Erratum: *J.Math.Phys.* 42, 2345 (2001)], [hep-ph/9910546](https://arxiv.org/abs/hep-ph/9910546). 7
- [41] Stavropoulos, D., Pestel, V., Aly, Z., Tzamariudaki, E. & Markou, C. Atmospheric neutrinos from the first KM3NeT/ORCA data and prospects for measuring the atmospheric neutrino flux. *PoS ICRC2021*, 1125 (2021). 7
- [42] Kalaczyński, P. KM3NeT/ORCA: status and perspectives for neutrino oscillation and mass hierarchy measurements. *PoS ICHEP2020*, 149 (2021). 2107.10593. 7
- [43] Agrawal, V., Gaisser, T., Lipari, P. & Stanev, T. Atmospheric neutrino flux above 1-GeV. *Phys. Rev. D* **53**, 1314–1323 (1996). [hep-ph/9509423](https://arxiv.org/abs/hep-ph/9509423). 7

-
- [44] Formaggio, J. & Zeller, G. From eV to EeV: Neutrino Cross Sections Across Energy Scales. *Rev. Mod. Phys.* **84**, 1307–1341 (2012). [1305.7513](#). [8](#)
- [45] Davidson, S., na Garay, C. P., Rius, N. & Santamaria, A. Present and future bounds on non-standard neutrino interactions **2003**, 011–011. [8](#)
- [46] Biggio, C., Blennow, M. & Fernández-Martínez, E. General bounds on non-standard neutrino interactions. *Journal of High Energy Physics* **2009**, 090 (2009). URL <https://dx.doi.org/10.1088/1126-6708/2009/08/090>. [8](#)
- [47] Fernandez-Martinez, E. Non-standard neutrino interactions. *PoS HQL2010*, 056 (2011). [8](#)
- [48] D’Olivo Saez, J. C., Lara, J. A. H., Romero, I. & Sampayo, O. A. Oscillation tomography study of Earth’s composition and density with atmospheric neutrinos. *Eur. Phys. J. C* **82**, 614 (2022). [2207.11257](#). [8](#), [13](#)
- [49] Wilks, S. S. The large-sample distribution of the likelihood ratio for testing composite hypotheses. *Ann. Math. Statist.* **9**, 60–62 (1938). URL <https://doi.org/10.1214/aoms/1177732360>. [9](#)